Enhancement of the Goos-Hänchen shift via chiral quantum-dot molecule systems

Muhammad Idrees,* Muhib Ullah, and Li-Gang Wang†
School of Physics, Zhejiang University, Hangzhou 310027, China

(Received 8 November 2022; revised 8 March 2023; accepted 26 June 2023; published 5 July 2023)

The role of a chiral quantum-dot molecule (QDM) system in controlling and enhancing the Goos-Hänchen (GH) shift is revealed here. The proposed setup is a four-level atomic system excited by incoherent pump and probe fields where the electron tunneling is prominent in affecting the GH shift upon the reflection and transmission of probe beams. The GH shifts in the chiral QDM system are calculated analytically by using stationary phase theory, whereas the dynamics of the quantum-dot system are derived by the density-matrix method. It is demonstrated that the GH shifts through transmission and reflection light beams are strongly influenced due to right-circularly polarized (RCP) and left-circularly polarized light. The GH shifts through RCP light are enhanced in the presence of chiral QDM systems, and these shifts could become either highly negative or highly positive, sensitively depending on the electron tunneling and chiral coefficients. This proposal can be viewed as a theoretical approach to the potential application of GH shifts in nano-optoelectronic sensors.

DOI: 10.1103/PhysRevA.108.013701

I. INTRODUCTION

In geometrical optics, it is generally known that the position of transmitted and reflected light beams can be shifted laterally. When a complete reflection occurs at the interface between two different media and is perpendicular to the path of propagation in the area containing both reflected and incident beams, the Goos-Hänchen (GH) shift takes place here between incident and reflected light beams [1]. This phenomenon relates to the GH shift reported experimentally by Goos and Hänchen [2,3]. The phenomenon was theoretically described using Renard's energy flux and Artmann's stationary phase techniques [4,5]. The GH shift is used to characterize the permittivity ε and permeability μ of different material media and to develop micrometer-scale surface plasmon resonance waveguide devices [6,7]. The negative GH shift at the boundary of left-handed and normal media was investigated by Berman [8] and Lakhtakia [9]. The lateral shift of a Gaussian light beam reflecting off a grounded slab having concurrently negative permeability and permittivity was explored by Kong *et al.* [10]. A method for achieving the modification of a probe beam's GH shifts using the control field and the fixed geometrical arrangement was put forward by Wang *et al.* [11]. Since then, a series of quantum-optics methods have been proposed to flexibly manipulate the GH shift of the reflected or transmitted probe fields, such as a multilevel system with electromagnetically induced transparency (EIT) [12], a four-level system governed by two external coherent beams [13], a cold and hot atomic medium [14], and cavity optomechanical systems [15]. Recently, using fractional dual fields as an excitation source, Ali *et al.* have proposed a GH shift for low-index metamaterials [16]. Similarly, using the Lorentz-Drude model, Nisar *et al.* presented the GH shift in a dielectric-magnetic dispersive system [17]. Likewise, Bibi *et al.* provided the GH shift analysis for a dielectric-chiral interface with noninteger dimensional regions [18]. Furthermore, Wu *et al.* introduced dual quasibound states in the continuum in compounded grating waveguide structures with a complete reflection for huge positive and negative GH shifts [19].

Alternatively, the optical characteristics of quantum wells and quantum dots (QDs) can be altered by interdot tunneling and external laser field interaction [20–22]. In an asymmetric double-QD configuration, Villas-Bôas *et al.* used Rabi oscillations to effectively control electron tunneling [23]. The concept of the quantum coherence phenomenon in a semiconductor QD was studied by Chow *et al.* [24]. It is widely understood that the electron tunneling and incoherent pump field in a QD system can significantly alter the optical characteristics of a QD medium [25]. Several further works have also investigated various optical phenomena in the quantum-dot molecule (QDM) governed by interdot tunneling, for example, entanglement and quantum-information transfer [26], four-wave mixing generation [27], transmission and reflection of pulses [28], optical bistability [29], and controlling the GH shift in a QD nanostructure [30]. Various parameters, including control field intensity, detuning, and electron tunneling, have been put forward for managing lateral shifts because of numerous proposals. As a result, it is worthwhile to investigate the modification and control of lateral shifts by modifying the different parameters of a scheme.

Motivated by the above studies, we propose a way to control and enhance GH shift, i.e., by using the right-circularly polarized (RCP) and left-circularly polarized (LCP) light fields in a chiral QDM system. It has been found that RCP light and LCP light exert a significant amount of impact on the GH shifts that occur in the transmission and reflection of a probe beam. The enhancement of GH shift via LCP and

*idreesoptics@yahoo.com
†lgwang@zju.edu.cn

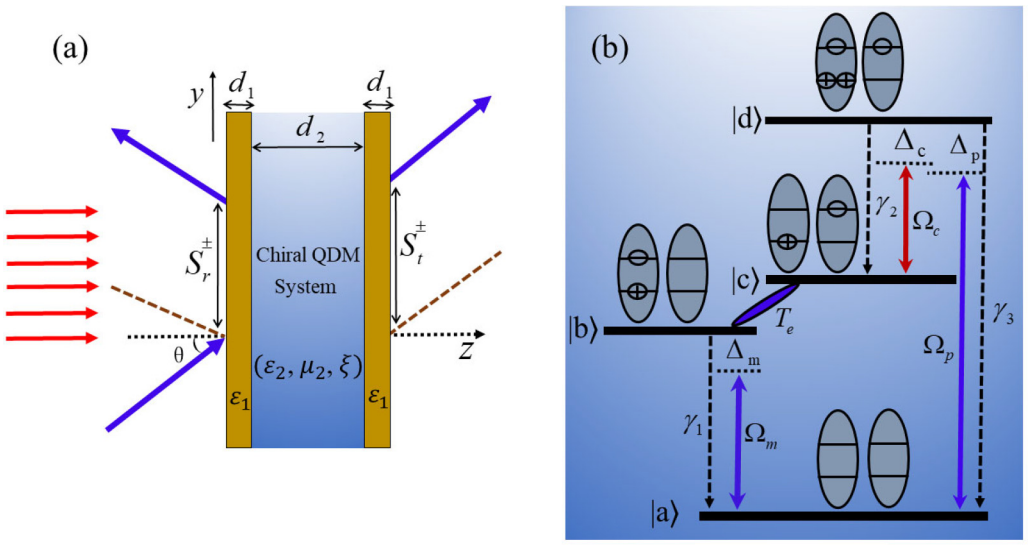

FIG. 1. (a) Schematic of a cavity containing a quantum-dot molecule (QDM) and (b) level configuration of the QDM system. The electron and hole are shown by ⊖ and ⊕, respectively. The $S_r^{\pm}$ and $S_t^{\pm}$ denote the lateral shifts of the reflected and transmitted probe beams.

RCP light becomes more vivid with the use of the chiral QDM system. It is also demonstrated that the GH shift can be either a large positive shift or a large negative shift, as influenced by the strength of the interdot tunneling and chirality coefficients at different incidence angles. Our proposed system can be viewed as a theoretical candidate for the creation of new nano-optoelectronic sensors.

II. SYSTEM MODEL AND ITS DYNAMICS

In this section, we examine a light beam called the probe that comes from the vacuum and strikes a cavity. The cavity holds a chiral quantum-dot medium with electric permittivity ε_2, magnetic permeability μ_2, and chirality coefficient ξ, while the free space has permittivity ε_o. The cavity consists of two dielectric slabs that have the same thickness d_1, and their permittivity is ε_1. Additionally, there is a chiral quantum system inside the cavity, which has thickness d_2. The setup is illustrated in Fig. 1(a). Figure 1(b) shows a uniform ensemble of structurally asymmetric quantum-dot molecules (QDMs), where each molecule is formed by the tightly spaced coupling of two quantum dots. To illustrate a practical scenario, we examine a side-to-side connection of two self-created (In,Ga)As/GaAs quantum dots that possess varying band configurations. A homogeneous group of QDMs made up of two dots, with a low density (5×10^7 cm^{-2}), can be created through a distinct mixture of molecular beam and atomic layer methods [31,32]. Each quantum dot (QD) typically has a lateral size of approximately 35 nm, and the thickness of the interdot barrier should be only a few nanometers (less than 8 nm) to enable significant electron tunneling between the dots. One might go for additional experimental information regarding the fabrication method in Ref. [33].

The chiral QD system has four energy levels, $|a\rangle$, $|b\rangle$, $|c\rangle$, and $|d\rangle$ [see Fig. 1(b)]. The ground state $|a\rangle$ indicates a level where two QDs are in the valance band. State $|b\rangle$ denotes the level at which an electron is driven to the conduction band in left QDs, thus resulting in an exciton. State $|c\rangle$ shows an electron transfer via interdot tunneling to the conduction band of the right QD, and thus an indirect exciton is created. Finally, state $|d\rangle$ expresses that the exciton is produced when an electron is excited to the right QD's conduction band. The magnetic field B with Rabi frequency Ω_m drives the transition between state $|a\rangle$ and state $|b\rangle$. The interdot tunneling strength T_e drives the transition between state $|b\rangle$ and state $|c\rangle$ and is responsible for the generation of an indirect exciton. The strong control field E_c with Rabi frequency Ω_c drives the transition between state $|c\rangle$ and state $|d\rangle$, whereas the weak probe field E_p with Rabi frequency Ω_p stimulates the transition between state $|a\rangle$ and state $|d\rangle$.

The Rabi frequency Ω_m in terms of the magnetic field is given as $\Omega_m = \mu B/\hbar$, where μ is the magnetic dipole moment and $\hbar$ is the reduced Planck's constant. Therefore the allowed transition $|a\rangle \rightarrow |b\rangle$ is a magnetic dipole transition. Magnetic dipole transitions are important in chiral QD systems because they are sensitive to the chirality of the environment and can lead to interesting optical properties. In the chiral QD system, the magnetic dipole transitions are enhanced due to the interaction between the electromagnetic field and the chiral environment. This enhancement can be described in terms of the chirality coefficient, which is a measure of the strength of the chiral response of the material. The chirality coefficient is related to the refractive index of left- and right-handed circularly polarized light as it passes through the material, and it can enhance the magnetic dipole transitions. Similarly, the Rabi frequencies Ω_c and Ω_p in terms of the electric field are given as $\Omega_c = \sigma E_c/\hbar$ and $\Omega_p = \sigma E_p/\hbar$, respectively, where σ is the electric dipole moment. Therefore the allowed transitions between states $|c\rangle \rightarrow |d\rangle$ and $|a\rangle \rightarrow |d\rangle$ are electric dipole transitions, which are more common than magnetic dipole transitions. The system's interaction Hamiltonian can be written as follows using the dipole approximation and rotating-wave approximation [32]:

$$H_I = -\hbar\big[\Omega_m e^{-i\Delta_m t}|a\rangle\langle b| + \Omega_p e^{-i\Delta_p t}|a\rangle\langle d| + \Omega_c e^{-i\Delta_c t}|d\rangle\langle c| + T_e|b\rangle\langle c| + \text{H.c.}\big], \quad (1)$$

where the quantity T_e denotes the interdot tunneling strength caused by a static electric field across states $|b\rangle$ and $|c\rangle$ and the term "H.c." represents the Hermitian conjugate. The parameters Δ_m, Δ_p, and Δ_c account for the detunings of the magnetic, probe, and control fields, respectively [see Fig. 1(b)]. The general quantum Liouville density-matrix equation can be expressed as follows [32,34]:

$$\dot{\rho} = -\frac{i}{\hbar}[H_I, \rho] - \frac{1}{2}\sum \gamma_j(\delta^\dagger\delta\rho + \rho\delta^\dagger\delta - 2\delta\rho\delta^\dagger), \quad (2)$$

where ρ represents the density operator of the system, H_I is the interaction Hamiltonian, γ_j $(j = 1, 2, 3)$ are the spontaneous decay rates, and $\delta^\dagger$ (δ) represents the raising (lowering) operator that describes all energy state transitions in the theoretical atomic model [see Fig. 1(b)]. By inserting Eq. (1) into Eq. (2), we obtain the density-matrix equations below:

$$\dot{\rho}_{ba} = \left[i\Delta_m + \tfrac{1}{2}(\gamma_1 + \gamma_3)\right]\rho_{ba} - i\Omega_m^*(\rho_{aa} - \rho_{bb}) + iT_e^*\rho_{ca} - i\Omega_p\rho_{bd}, \quad (3)$$

$$\dot{\rho}_{ca} = \left[i(\Delta_c - \Delta_p) + \tfrac{1}{2}(\gamma_1 + \gamma_2 + \gamma_3)\right]\rho_{ca} + i\Omega_c^*\rho_{da} + iT_e^*\rho_{ba} - i\Omega_m\rho_{cb} - i\Omega_p\rho_{cd}, \quad (4)$$

$$\dot{\rho}_{da} = \left[i\Delta_p + \tfrac{1}{2}(\gamma_1 + \gamma_3)\right]\rho_{da} + i\Omega_c\rho_{ca} - i\Omega_p^*(\rho_{aa} - \rho_{dd}) - i\Omega_m\rho_{db}. \quad (5)$$

These equations characterize the evolution of the system as influenced by laser beams and electron tunneling strength coupling. We have investigated the enhancement of the GH shift by using the chiral QDM system (which can be defined as a medium in which the electric polarization is coupled to the magnetic field H of electromagnetic radiation and the magnetization M is coupled to the electric field E) that can be expressed as [35,36]

$$P = \frac{\xi_{EH}}{c}H + \varepsilon_0\chi_e E, \quad (6)$$

$$M = \chi_m H + \frac{\xi_{HE}}{\mu_0 c}E, \quad (7)$$

where ξ_{EH} and ξ_{HE} represent the chirality coefficients, ε_0 (μ_0) represents the permittivity (permeability) of the vacuum, and c is the speed of light. By solving the above equations, the following chirality coefficients, electric susceptibility χ_e, and magnetic susceptibility χ_m are calculated [36]:

$$\chi_e = \frac{\sigma^2}{\epsilon_0\hbar}\left[\frac{\beta_2(\hbar - N\mu^2\mu_0\beta_3) + N\mu^2\mu_0\beta_1\beta_4}{\hbar - N\mu^2\mu_0\beta_3}\right], \quad (8)$$

$$\chi_m = \frac{N\mu^2\mu_0\beta_3}{\hbar - N\mu^2\mu_0\beta_3}, \quad (9)$$

$$\xi_{EH} = \frac{Nc\mu\mu_0\sigma^2\beta_1}{\hbar - N\mu^2\mu_0\beta_3}, \quad (10)$$

$$\xi_{HE} = \frac{Nc\mu\mu_0\sigma\beta_4}{\hbar - N\mu^2\mu_0\beta_3}, \quad (11)$$

where

$$\beta_1 = -\frac{i(A_1A_2 + T_e^2 + A_1\Omega_c[-i\cos(\theta_c) + \sin(\theta_c)])}{A_1(A_2A_3 + \Omega_c^2) + A_3T_e^2}, \quad (12)$$

$$\beta_2 = \frac{-e^{i\theta_c}\Omega_c(A_1 - iT_e) + i(A_1A_2 + T_e^2)}{A_1(A_2A_3 + \Omega_c^2) + A_3T_e^2}, \quad (13)$$

$$\beta_3 = \frac{T_e[-A_3 + i\Omega_c\cos(\theta_c) + \Omega_c\sin(\theta_c)]}{A_1(A_2A_3 + \Omega_c^2) + A_3T_e^2}, \quad (14)$$

$$\beta_4 = \frac{i(A_2A_3 + \Omega_c^2 - iA_3T_e + e^{i\theta_c}\Omega_cT_e)}{A_1(A_2A_3 + \Omega_c^21) + A_3T_e^2}. \quad (15)$$

$A_1 = i\Delta_m + \frac{1}{2}(\gamma_1 + \gamma_3)$, $A_2 = i(\Delta_c - \Delta_p) + \frac{1}{2}(\gamma_1 + \gamma_2 + \gamma_3)$, and $A_3 = i\Delta_p + \frac{1}{2}(\gamma_1 + \gamma_3)$. The σ represents the electric dipole moment, μ is the magnetic dipole moment, N stands for the number of atoms per volume (atomic density), and θ_c is the phase of the control field.

A chiral QD medium is a material that exhibits chirality, which has different properties for LCP and RCP light. The optical properties of a chiral QD system can be described in terms of the chirality coefficients $(\xi_{EH(HE)})$, magnetic permeability (μ_2), electric permittivity (ε_2), and the refractive index $(n_r^{(\pm)})$. The chirality coefficient is a measure of the strength of the chiral response of the material, such that a larger chirality coefficient indicates a stronger chiral response in the optical properties of LCP and RCP light. The magnetic permeability of a chiral medium describes the material's response to an applied magnetic field and can affect the propagation of light through the material. In a chiral QD system, the refractive index for left- and right-circularly polarized light is given by [37,38]

$$n_r^{(\pm)} = \sqrt{(1+\chi_e)(1+\chi_m) - \frac{(\xi_{EH} + \xi_{HE})^2}{4}} \pm \frac{i}{2}(\xi_{EH} - \xi_{HE}), \quad (16)$$

where $n_r^{(+)}$ denotes the complex refractive index for the RCP light beam and $n_r^{(-)}$ denotes the complex refractive index for the LCP light beam. Quantitatively speaking, when the quantum-dot system satisfies the condition $\xi_{EH(HE)} \neq 0$, the system is assumed to be a chiral quantum-dot system; otherwise, it is assumed to be a nonchiral quantum-dot system with $\xi_{EH(HE)} = 0$. The chiral quantum-dot system contributes additional chirality coefficient terms to refractive indices in addition to permeability $(\mu_2 = 1 + \chi_m)$ and permittivity $(\varepsilon_2 = 1 + \chi_e)$. Consider an incident probe beam that interacts with the chiral QD system making an angle θ along the z axis [39]. Such a QD system is also used for the observation of superluminal light propagation and control of the probe absorption via electron tunneling strength and incoherent pumping field [21,25]. The GH shifts for both reflected and transmitted probe beams can be calculated with the help of the stationary phase theory [4,5], as follows:

$$S_{(r,t)}^{\pm} = -\frac{\lambda}{2\pi}\frac{d\phi_{r,t}}{d\theta}, \quad (17)$$

where $S_{(r,t)}^{\pm}$ are the lateral shifts in both reflected and transmitted probe beams for the RCP and LCP light and $\phi_{r,t}$ corresponds to the phase of the complex reflection $r(k_y, \omega_p)$ or transmission $t(k_y, \omega_p)$ coefficients. Therefore one can describe the probe beams for the lateral shift or the GH shift as [40]

$$S_r^{\pm} = -\frac{\lambda}{2\pi|r(k_y,\omega_p)|^2}\left[\mathrm{Re}[r(k_y,\omega_p)]\frac{\partial\,\mathrm{Im}[r(k_y,\omega_p)]}{\partial\theta} - \mathrm{Im}[r(k_y,\omega_p)]\frac{\partial\,\mathrm{Re}[r(k_y,\omega_p)]}{\partial\theta}\right], \quad (18)$$

$$S_t^{\pm} = -\frac{\lambda}{2\pi |t(k_y,\omega_p)|^2}\left[\mathrm{Re}[t(k_y,\omega_p)]\frac{\partial\,\mathrm{Im}[t(k_y,\omega_p)]}{\partial\theta} - \mathrm{Im}[t(k_y,\omega_p)]\frac{\partial\,\mathrm{Re}[t(k_y,\omega_p)]}{\partial\theta}\right], \quad (19)$$

where k_y represents the y component of the wave vector k, ω_p is the angular frequency of the probe field ($\omega_p = 2\pi c/\lambda$), λ is the corresponding wavelength of the probe field, and θ represents the incident angle of the probe field with the z axis [see Fig. 1(a)]. We use the standard characteristic matrix technique to figure out the transmission coefficient $t(k_y,\omega_p)$ and reflection coefficient $r(k_y,\omega_p)$ of the probe beam passing through the cavity.

III. RESULTS AND DISCUSSION

Here we discuss in detail the GH shifts in both transmitted and reflected probe beams for LCP and RCP light via chiral and nonchiral QD systems. In addition, we elaborate on how electron tunneling and magnetic field detuning influence the behavior of GH shifts.

In the context of GH shift via atomic systems, we choose the decay rate of excited states as $\gamma = 1$ MHz (the natural linewidth of atomic systems), and it is convenient to scale all the other parameters with γ in the given calculations for the better understanding of the reader [11,12]. The GH shifts ($S_{r,t}^{\pm}$) in both reflected and transmitted probe beams for RCP light as a function of incidence angle θ are plotted for various values of electron tunneling strength in a nonchiral QD system ($\xi_{EH(HE)} = 0$), as shown in Figs. 2(a) and 2(b). We have observed small positive GH shifts in the transmitted probe beam (blue curve) and comparatively large negative GH shifts in the reflected probe beams (red curve) for RCP light at $T_e = 2\gamma$ [see Fig. 2(a)]. The maximum positive GH shift in the transmitted probe beam ($S_t^+ = 1.6\lambda$) is observed at the incident angle $\theta = 1.0$ rad, while the maximum negative GH shift in the reflected probe beam ($S_r^+ = -4.2\lambda$) is observed at the incident angle $\theta = 0.68$ rad for RCP light [see Fig. 2(a)]. When T_e is raised to 4γ, both S_t^+ (blue curve) and S_r^+ (red curve) increase [see Fig. 2(b)]. The maximum positive GH shift in the transmitted probe beam is increased to $S_t^+ = 1.8\lambda$, at the incident angle $\theta = 1.0$ rad, while the maximum negative GH shift in the reflected probe beam is increased to $S_r^+ = -7.0\lambda$, at the incident angle $\theta = 0.68$ rad [see Fig. 2(b)]. Furthermore, the GH shifts exhibited by LCP light within a nonchiral medium are identical to those of RCP light.

In a chiral QD system ($\xi_{EH(HE)} \neq 0$), the GH shifts in both reflected and transmitted probe beams for RCP and LCP light ($S_{r,t}^{\pm}$) as a function of incidence angle θ are plotted for various values of electron tunneling strength, as illustrated in Figs. 3(a)–3(d). In the chiral QD system, we have observed large positive GH shifts in the transmitted probe beam (blue curve) and comparatively smaller negative GH shifts in the reflected probe beams (red curve) for RCP light at $T_e = 2\gamma$ [see Fig. 3(a)]. The maximum positive GH shift in the transmitted probe beam ($S_t^+ = 13.1\lambda$) and maximum negative GH shift in the reflected probe beam ($S_r^+ = -6.0\lambda$) are observed for RCP light at the incident angle $\theta = 0.670$ rad [see Fig. 3(a)]. When T_e is raised to 4γ, both S_t^+ (blue curve) and S_r^+ (red curve) increase [see Fig. 3(b)]. The maximum positive GH shift in the transmitted probe beam for RCP light is increased to $S_t^+ = 22.1\lambda$, while the maximum negative GH shift in the reflected probe beam for RCP light is increased to $S_r^+ = -16.0\lambda$, at the incident angle $\theta = 0.670$ rad [see Fig. 3(b)]. In contrast, we have observed small negative GH shifts in the transmitted probe beam (blue curve) and comparatively large positive GH shifts in the reflected probe beams (red curve) for LCP light at $T_e = 2\gamma$ [see Fig. 3(c)]. The maximum negative GH shift in the transmitted probe beam ($S_t^- = -2.1\lambda$) is observed at the incident angle $\theta = 1.18$ rad, while the maximum positive GH shift in the reflected probe beam ($S_r^- = 5.9\lambda$) is observed at the incident angle $\theta = 0.670$ rad, for LCP light [see Fig. 3(c)]. Furthermore, when T_e is raised to 4γ, both S_t^- (blue curve) and S_r^- (red curve) increase [see Fig. 3(d)]. The maximum negative GH shift in the transmitted probe beam for LCP light is increased to $S_t^- = -3.1\lambda$ at the incident angle $\theta = 1.18$ rad, and the maximum positive GH shift in the reflected probe beam for LCP light is increased to $S_r^- = 12.1\lambda$, at the incident angle $\theta = 1.46$ rad [see Fig. 3(d)]. It is found that the QDM system gets more transparent and the absorption varies when the strength of the interdot electron tunneling is increased, resulting in larger negative and positive shifts at specific incident angles. Similarly, the difference in refractive indices for RCP and LCP light leads to differential GH shifts for the two polarizations. Specifically, RCP light experiences larger GH shifts than LCP light in both reflected and transmitted probe beams in a chiral medium. This is because the interaction

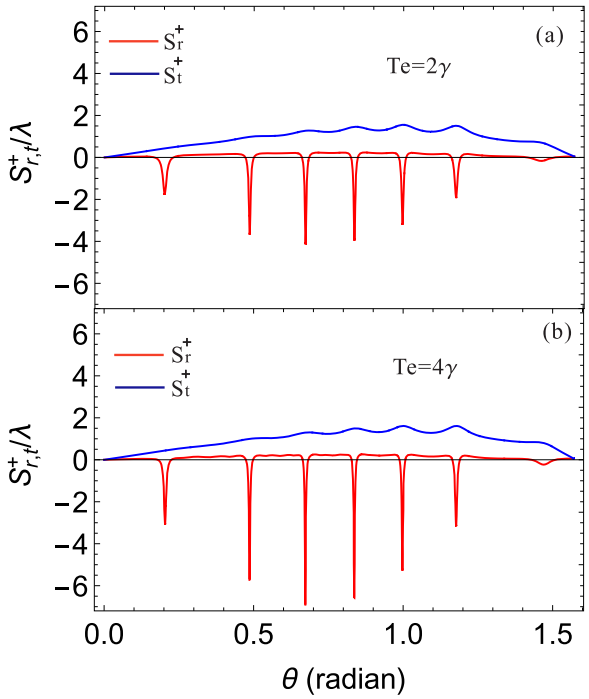

FIG. 2. (a) and (b) GH shift in reflection and transmission of RCP light vs incident angle θ in a nonchiral medium ($\xi_{EH(HE)} = 0$) under different values of interdot tunneling strength T_e. The system parameters used are $\gamma = 1$ MHz, $\gamma_1 = \gamma_2 = \gamma_3 = 0.1\gamma$, $\Omega_c = 6\gamma$, $\Delta_c = \Delta_p = \Delta_m = 0.1\gamma$, $\sigma = 1.6\times10^{-19}$ C m, $\mu = 0$ A m^2, $\lambda = 500$ nm, $\hbar = 1.05\times10^{-34}$ J s, $c = 3\times10^8$ m/s, $\theta_c = \pi$, $d_1 = 0.6$ μm, $d_2 = 1.2$ μm, $\epsilon_0 = 8.85\times10^{-12}$ F/m, and $\epsilon_1 = 2.22$.

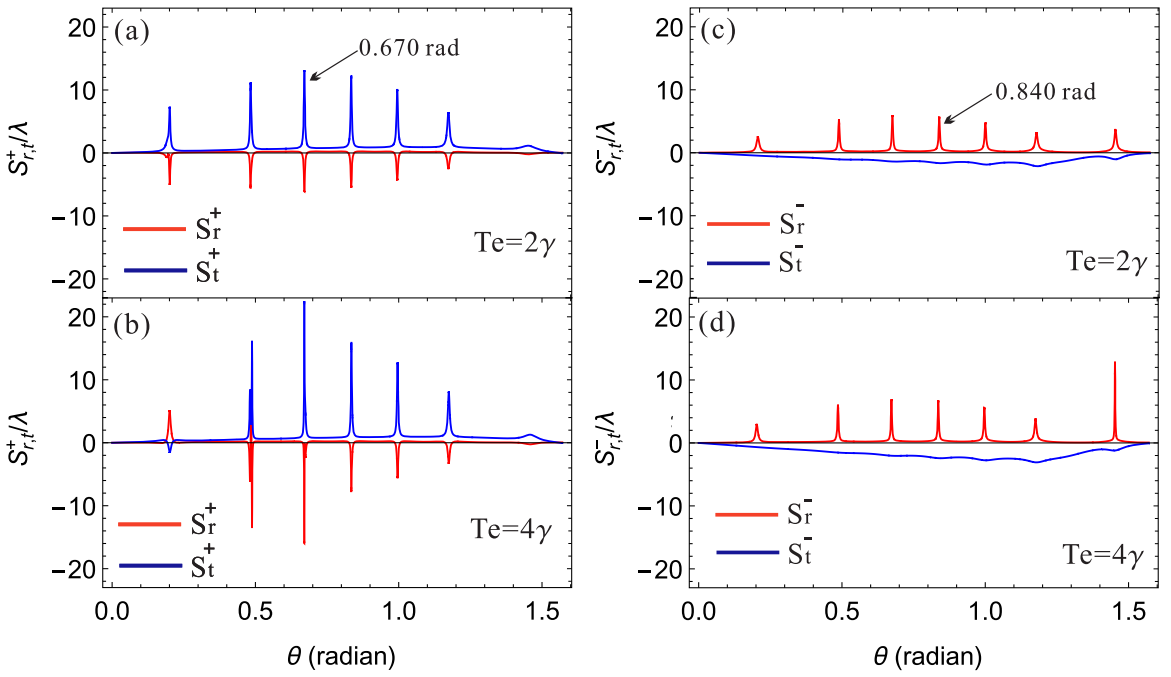

FIG. 3. GH shift in reflection and transmission of (a) and (b) RCP light and (c) and (d) LCP light plotted against the incident angle θ in a chiral medium ($\xi_{EH(HE)} \neq 0$) under different values of interdot tunneling strength T_e. The system parameters used are as follows: $\mu = 1.16\times10^{-21}$ A m^2, and all the other parameters are the same as in Fig. 2.

between RCP light and the chiral medium is stronger due to the matching of the handedness of the light polarization and the chiral nature of the medium. Therefore the GH shift increases in a chiral medium compared with a nonchiral medium.

In Figs. 4(a) and 4(b), the GH shifts in both reflected and transmitted probe beams for the RCP and LCP light ($S^{\pm}_{r,t}$) as a function of Δ_m/γ are plotted for various values of incidence angle θ. Figure 4(a) depicts RCP curves plotted at $\theta = 0.670$ rad, whereas Fig. 4(b) depicts LCP curves plotted at $\theta = 0.840$ rad. In this case, we have observed positive GH shifts in the transmitted probe beam (blue dashed curve) and negative GH shifts in the reflected probe beams (red curve) for RCP light at $T_e = 2\gamma$ [see Fig. 4(a)]. The GH shift in the transmitted probe beam is 13.1λ, and the GH shift in the reflected probe beam is -6.0λ at $\Delta_m = 0.1\gamma$. In contrast, we have observed negative GH shifts in the transmitted probe beam (blue dashed curve) and positive GH shifts in the reflected probe beams (red curve) for LCP light at $T_e = 2\gamma$ [see Fig. 4(b)]. The GH shift in the transmitted probe beam is -2.0λ while the GH shift in the reflected probe beam is 5.9λ at $\Delta_m = 0.1\gamma$.

In Figs. 5(a)–5(d), the imaginary and real parts of magnetic and electric susceptibilities are plotted as a function of the magnetic field detuning Δ_m in a chiral QD system. Here we see that the electric and magnetic susceptibilities are strongly dependent on the interdot tunneling strength T_e. The function of susceptibility is somewhat complex and is composed of two components, namely, the imaginary component and the real component. Both the imaginary component and the real component have a direct relationship to the spectrum of absorption and its dispersion, accordingly. Here we have observed the imaginary (Im[χ_m]) and real parts (Re[χ_m]) of magnetic susceptibility in Figs. 5(a) and 5(b), respectively. At $T_e = 2\gamma$, we have examined a large absorption and small anomalous dispersion (red curve) as shown in Figs. 5(a) and 5(b),

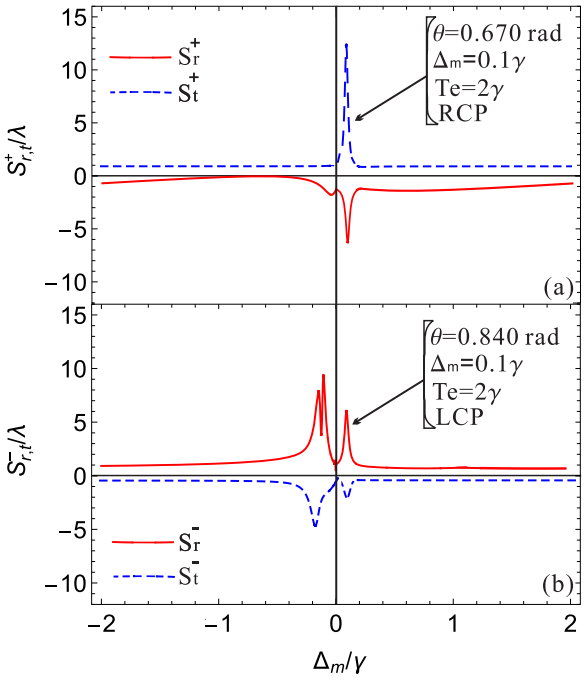

FIG. 4. GH shifts in both reflected and transmitted probe beams for RCP and LCP light ($S^{\pm}_{r,t}$) as a function of detuning Δ_m in chiral medium ($\xi_{EH(HE)} \neq 0$). (a) GH shift in reflection and transmission probe beams for RCP light at $\theta = 0.670$ rad, and (b) GH shift in reflection and transmission probe beams for LCP light at $\theta = 0.840$ rad. The other parameters are the same as in Fig. 2.

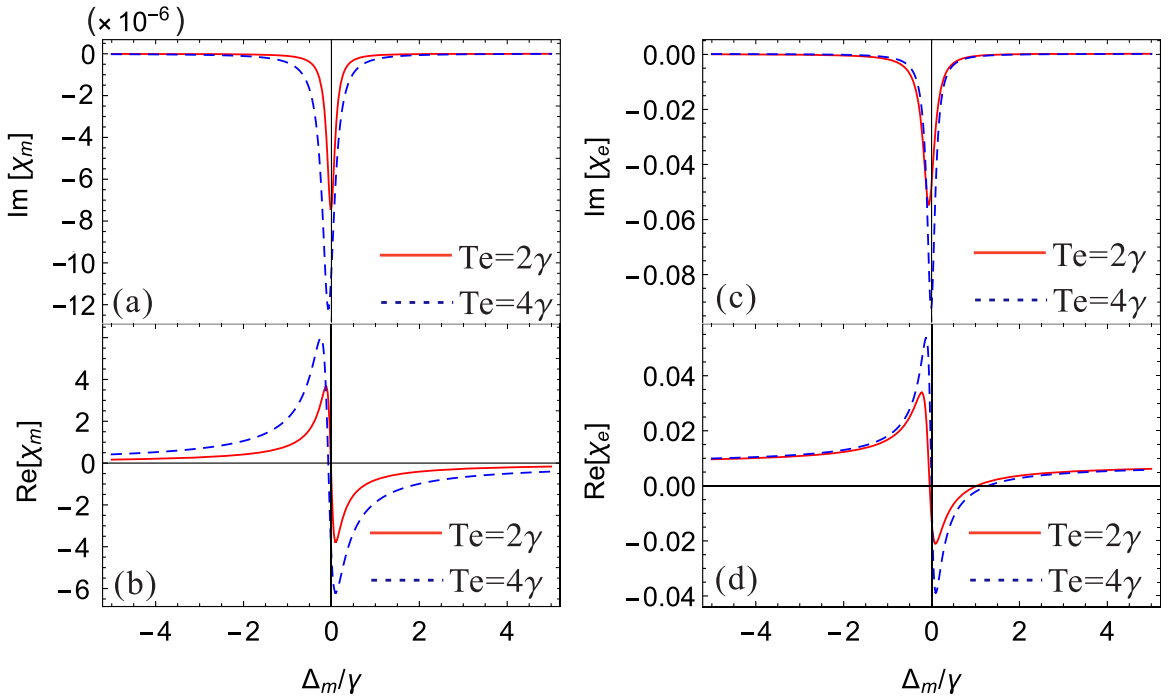

FIG. 5. (a) and (b) Imaginary and real parts of magnetic susceptibility and (c) and (d) imaginary and real parts of electric susceptibility vs Δ_m/γ under different values of T_e. Red curve, $T_e = 2\gamma$; blue dashed curve, $T_e = 4\gamma$. All the other parameters are the same as in Fig. 2.

respectively. When interdot tunneling strength T_e is increased to 4γ, the absorption decreases, and the anomalous dispersion (blue dashed curve) increases as shown in Figs. 5(a) and 5(b), respectively. Likewise, we have also observed the imaginary ($\mathrm{Im}[\chi_e]$) and real parts ($\mathrm{Re}[\chi_e]$) of electric susceptibility in Figs. 5(c) and 5(d), respectively. We examined a large absorption and small anomalous dispersion (red curve) at $T_e = 2\gamma$, as depicted in Figs. 5(c) and 5(d), respectively. Similar to this, as illustrated in Figs. 5(c) and 5(d), when interdot tunneling strength T_e is increased to 4γ, the absorption decreases, and the anomalous dispersion increases (blue dashed curve). It is found that in the QDM system, the transmitted and reflected probe beam GH shifts are seen to be reduced by the strong absorption, while the transmitted and reflected probe beam GH shifts are thus found to be enhanced by the small absorption.

IV. CONCLUSIONS

In conclusion, we have proposed a method to use a chiral QD system inside a cavity to control the GH shifts in both reflected and transmitted probe beams for RCP and LCP light. It is observed that the strength of the interdot electron tunneling and magnetic field detuning strongly affects the behavior of the GH shift. It is demonstrated that the GH shifts in transmission and reflection light beams show different behavior for the RCP and LCP light. In the presence of a chiral QD system, the GH shifts are enhanced under RCP light. Furthermore, at different angles of incidence, the lateral shift can become a large positive shift or a large negative shift, which is influenced by the strength of the interdot tunneling of electrons and the chiral coefficients. Our proposed system can be viewed as a theoretical approach to the creation of new nano-optoelectronic sensors and encourages experimental research on GH shifts.

ACKNOWLEDGMENT

This work was supported by the National Natural Science Foundation of China (NSFC; Grant No. 11974309).

[1] J. Picht, Ann. Phys. (Berlin) **395**, 433 (1929).
[2] F. Goos and H. Hänchen, Ann. Phys. (Berlin) **436**, 333 (1947).
[3] F. Goos and H. L. Hänchen, Ann. Phys. (Berlin) **440**, 251 (1949).
[4] R. H. Renard, J. Opt. Soc. Am. **54**, 1190 (1964).
[5] E. F. F. Chladni, Ann. Phys. (Berlin) **2**, 87 (1799).
[6] X. Hu, Y. Huang, W. Zhang, D.-K. Qing, and J. Peng, Opt. Lett. **30**, 899 (2005).
[7] G-Y. Oh, D. G. Kim, and Y. W. Choi, Opt. Express **17**, 20714 (2009).
[8] P. R. Berman, Phys. Rev. E **66**, 067603 (2002).
[9] A. Lakhtakia, Electromagnetics **23**, 71 (2003).
[10] J. A. Kong, B.-I. Wu, and Y. Zhang, Appl. Phys. Lett. **80**, 2084 (2002).
[11] L.-G. Wang, M. Ikram, and M. S. Zubairy, Phys. Rev. A **77**, 023811 (2008).
[12] Ziauddin, S. Qamar, and M. S. Zubairy, Phys. Rev. A **81**, 023821 (2010).
[13] J.-N. Su, W.-W. Deng, and G.-X. Li, Acta Phys. Sin. **61**, 144210 (2012).

[14] H. Iqbal, M. Idrees, M. Javed, B. A. Bacha, S. Khan, and S. A. Ullah, J. Russ. Laser Res. **38**, 426 (2017).
[15] M. Ullah, A. Abbas, J. Jing, and L.-G. Wang, Phys. Rev. A **100**, 063833 (2019).
[16] K. Ali, A. A. Syed, W. I. Waseer, and Q. A. Naqvi, Optik **243**, 167501 (2021).
[17] M. Nisar, M. Saghir, A. Shahzad, W. I. Waseer, and Q. A. Naqvi, Optik **262**, 169273 (2022).
[18] F. Bibi, M. A. Ashraf, W. I. Waseer, and Q. A. Naqvi, Eur. Phys. J. Plus **137**, 288 (2022).
[19] F. Wu, M. Luo, J. Wu, C. Fan, X. Qi, Y. Jian, D. Liu, S. Xiao, G. Chen, H. Jiang, Y. Sun, and H. Chen, Phys. Rev. A **104**, 023518 (2021).
[20] H. Schmidt, D. E. Nikonov, K. L. Campman, K. D. Maranowski, A. C. Gossard, and A. Imamoğlu, Laser Phys. **9**, 797 (1999).
[21] Z. Wang, Ann. Phys. (Amsterdam) **326**, 340 (2011).
[22] L. A. Openov, Phys. Rev. B **60**, 8798 (1999).
[23] J. M. Villas-Bôas, A. O. Govorov, and S. E. Ulloa, Phys. Rev. B **69**, 125342 (2004).
[24] W. W. Chow, H. C. Schneider, and M. C. Phillips, Phys. Rev. A **68**, 053802 (2003).
[25] M. Mahmoudi and M. Sahrai, Physica E (Amsterdam) **41**, 1772 (2009).
[26] X.-Y. Lü, J. Wu, L. L. Zheng, and Z. M. Zhan, Phys. Rev. A **83**, 042302 (2011).
[27] A. Sitek and P. Machnikowski, Phys. Status Solidi C **6**, 492 (2009).
[28] R. Nasehi, M. Mahmoudi, and M. Sahrai, Laser Phys. **26**, 115202 (2016).
[29] A. Vafafard, S. Goharshenasan, N. Nozari, A. Mortezapour, and M. Mahmoudi, J. Lumin. **134**, 900 (2013).
[30] R. Nasehi, S. H. Asadpour, H. R. Soleimani, and M. Mahmoudi, Chin. Phys. Lett. **33**, 014204 (2016).
[31] G. J. Beirne, C. Hermannstäter, L. Wang, A. Rastelli, O. G. Schmidt, and P. Michler, Phys. Rev. Lett. **96**, 137401 (2006).
[32] M. Mahdavi, Z. A. Sabegh, M. Mohammadi, M. Mahmoudi, and H. R. Hamedi, Phys. Rev. A **101**, 063811 (2020).
[33] G. J. Beirne, C. Hermannstdter, L. Wang, A. Rastelli, E. Mller, O. G. Schmidt, and P. Michler, Proc. SPIE **6471**, 647104 (2007).
[34] M. Scully and M. S. Zubairy, *Quantum Optics* (Cambridge University Press, Cambridge, 1997).
[35] J. B. Pendry, Science **306**, 1353 (2004).
[36] C. Monzon and D. W. Forester, Phys. Rev. Lett. **95**, 123904 (2005).
[37] J. Kästel, M. Fleischhauer, S. F. Yelin, and R. L. Walsworth, Phys. Rev. Lett. **99**, 073602 (2007).
[38] D. E. Sikes and D. D. Yavuz, Phys. Rev. A **82**, 011806(R) (2010).
[39] M. R. Mehmannavaz, R. Nasehi, H. Sattari, and M. Mahmoudi, Superlattices Microstruct. **75**, 27 (2014).
[40] L. G. Wang, H. Chen, and S. Y. Zhu, Opt. Lett. **30**, 2936 (2005).